Family of anisotropic spin glasses math xmlns="http://www.w3.org/1998/Math/MathML">mrow>msub>mi>Ba/mi>mrow>mn>1/mn>mtext>–/mtext>mi>x/mi>/mrow>/msub>msub>mi>La/mi>mrow>mn>1/mn>mo>+/mo>mi>x/mi>/mrow>/msub>mi>Mn/mi>msub>mi mathvariant="normal">O/mi>mrow>mn>4/mn>mo>+/mo>mi>δ/mi>/mrow>/msub>/mrow>/math>

Mirela Dragomir, Iztok Arčon, Paul A. Dube, Jeremiah C. Beam, Andrew P. Grosvenor, Graham King, and John E. Greedan

Phys. Rev. Materials **5**, 074403 — Published 9 July 2021

DOI: 10.1103/PhysRevMaterials.5.074403

A family of anisotropic spin glasses, $Ba_{1-x}La_{1+x}MnO_{4+\delta}$

Mirela Dragomir, [*a,b,c] Iztok Arčon,[d, e] Paul A. Dube,[b] Jeremiah C. Beam,[f] Andrew P. Grosvenor,[f] Graham King,[g] John E. Greedan[a,b]

[a] *Department of Chemistry and Chemical Biology, McMaster University, Hamilton, ON L8S 4M1, Canada*
[b] *Brockhouse Institute for Materials Research, McMaster University, Hamilton, ON L8S 4M1, Canada*
[c] *Electronic Ceramics Department, Jožef Stefan Institute, Jamova cesta 39, 1000 Ljubljana, Slovenia*
[d] *Laboratory of Quantum Optics, University of Nova Gorica, 5000 Nova Gorica, Slovenia*
[e] *Department of Low and Intermediate Energy Physics, Jožef Stefan Institute, Ljubljana 1000, Slovenia; Email: mirela.dragomir@ijs.si*
[f] *Department of Chemistry, University of Saskatchewan, Saskatoon, SK S7N 5C9, Canada*
[g] *Canadian Light Source, 44 Innovation Blvd., Saskatoon, SK S7N 2V3, Canada*

The synthesis, structural, and magnetic characterization of the series, $Ba_{1-x}La_{1+x}MnO_{4+\delta}$ ($0 \leq x \leq 0.5$) with the K_2NiF_4–type structure is reported. We previously found that $x = 0.2$ member exhibits the very rare anisotropic spin glass behaviour with only the *c*-axis spin component freezing below T_g. Here we show that each member of the $Ba_{1-x}La_{1+x}MnO_{4+\delta}$ ($0 \leq x \leq 0.4$) series exhibits the same spin glass behaviour. Moreover, T_g, varies with x, reaching a maximum of 26.4(4) K for $x = 0.20$ compared with 19.2(2) K for $x = 0$. The spin glass behaviour was confirmed by both dc and ac magnetic susceptibility measurements. No long-range magnetic order was found down to 2 K. All series members adopt the *I4/mmm* space group and subtle structural transformations occur with increasing La content. The unit cell volume contracts for $0.0 < x < 0.3$ and expands for $0.3 < x \leq 0.5$. Similar behaviour is seen for the equatorial Mn-O bonds in the Mn-O octahedron while the axial Mn-O distances increase to $x \sim 0.3$ but remain unchanged for higher x. XANES analysis revealed that the oxidation state of Mn in the $Ba_{1-x}La_{1+x}MnO_{4+\delta}$ samples varies with x: for $x \leq 0.2$ Mn is in +3.0(1) oxidation state only, while for $x > 0.2$ a mixed +2/+3 oxidation state was found. Therefore, for the charge balance, samples with $x \leq 0.2$ contain excess oxygen as an interstitial species, while for $x > 0.2$, the structure cannot sustain any more interstitial oxygen and the La excess is accommodated through the reduction of some Mn^{3+} to Mn^{2+}. Based on the oxidation state of Mn, the possible origins of the spin-glass magnetism in the $Ba_{1-x}La_{1+x}MnO_{4+\delta}$ series are discussed.

I. INTRODUCTION

Manganese oxides with the perovskite structure, such as $A_{1-x}A'_xMnO_3$, where A and A′ are Group 2 and Group 3 elements, respectively, are extremely interesting materials that have attracted massive attention due to their magnetoresistive properties which make them potential candidates for magnetic storage devices [1,2]. There are two viable approaches to tune the

electrical response to the magnetic field and improve the magnetorestrictive properties: (i) by chemical substitution on the A-site as above and/or (ii) by synthesising variants of the perovskite structure by adding a controlled number of MnO_2 sheets. For example, by inserting a rock-salt type layer every *n* MnO_2 sheets, the perovskite-type structure $(La,A)MnO_3$ transforms into layered structures, $(La,A)_{n+1}Mn_nO_{3n+1}$. These are called Ruddlesden-Popper (RP) phases with *n* being an integer from 0 to ∞. The *n* = 1 member of the RP phases is in fact the K_2NiF_4-type structure (**Figure 1a**) and compounds adopting this structure exhibit very interesting but different properties than the original one. Compounds such as $(La,A)_2Mn_2O_7$ result when *n* = 2 (**Figure 1c**) whose magnetic properties begin to resemble the starting perovskite compound [3]. Finally, the pure perovskite structure results when the number of sheets is *n* = ∞ (**Figure 1d**).

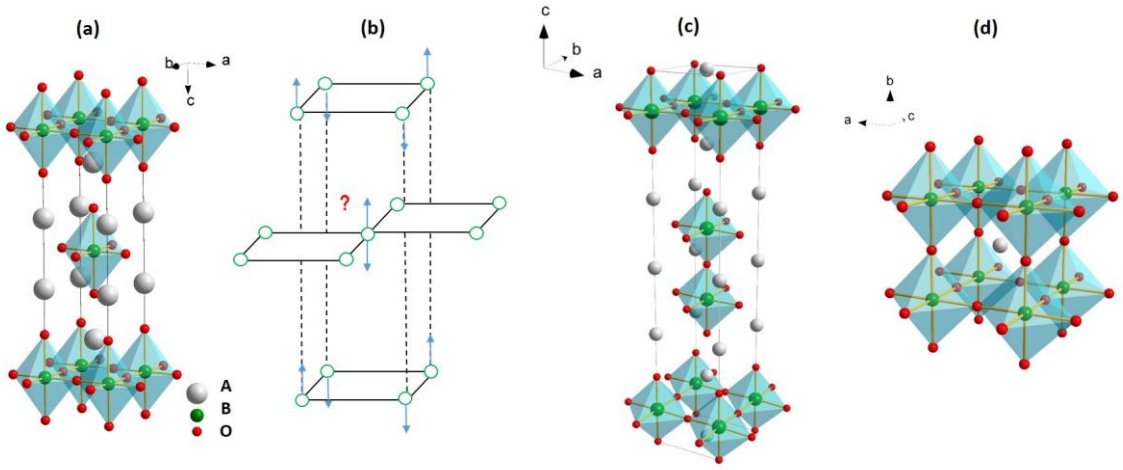

Figure 1 Ruddlesden-Popper phases: **(a)** with *n* = 1: A_2BO_4, or the K_2NiF_4 structure-type where the individual rock-salt and perovskite layers are illustrated and the body-centred magnetic sublattice **(b)** consisting of square planar layers and the condition for magnetic frustration; **(c)** with *n* = 2, $A_3B_2O_7$ structure; **(d)** with *n* = ∞, perovskite structure, ABO_3.

A K_2NiF_4–type compound was first reported in 1892 while the first structural characterisation was done almost concomitantly by Baltz in 1953 [4] and by Brehler in 1954 [5]. This structure-type mainly adopts the tetragonal *I*4/*mmm* space group. Here, the coordination number (C.N.) of the A-site cation is reduced to 9 due to the intergrowth with the perovskite layer. The B-site is occupied by a transition metal which, if of Jahn-Teller type, can experience an enhancement of the tetragonal distortion. Moreover, due to the large interstitial sites between the A and B-site cations, additional anions could be accommodated at the interface [6,7,8]. This structure-type has been recognized as the archetype structure for low dimensional magnetism with the magnetic sublattice consisting of square-planar layers which

are stacked in such an arrangement that magnetic ions located in adjacent layers are translated by a vector $\boldsymbol{t}$ = (½ ½ ½), which give rise to a body-centred tetragonal cell (**Figure 1b**). When the intraplanar magnetic ions are in an antiferromagnetic arrangement, the interplanar coupling becomes frustrated, leading to 2D magnetism. Examples of such compounds include: $SrLaMnO_4$ [9,10,11], $SrLaCrO_4$ [12], $SrLaFeO_4$ [13], La_2NiO_4 [14], $CaYCrO_4$ [15], and so on.

The magnetic properties of $SrLaMnO_4$ have been well studied [9,10,11] and it is known that an AF ordering in this compound establishes below T_N = 128 K. The La-rich compounds $Sr_{1-x}La_{1+x}MnO_{4+\delta}$ also show two-dimensional antiferromagnetic spin correlations and long-range antiferromagnetic order but with a lower T_N [16,17]. Quite surprisingly, the Ba analogues, $BaLaMnO_4$ and $Ba_{0.8}La_{1.2}MnO_{4.1}$ show no long-range magnetic correlations but a random freezing of spins below T_g of about 19 K and 26 K, respectively [16,18]. Moreover, magnetic measurements on $Ba_{0.8}La_{1.2}MnO_{4.1}$ crystal showed that only the *c* component of the spin freezes while the others remain dynamic down to 2 K [16]. This anisotropic spin glass behaviour is exceedingly rare, with only one other well-documented example in the literature, Fe_2TiO_5 [19].

This study concerns the magnetic properties of $BaLaMnO_4$ and its La-excess series, $Ba_{1-x}La_{1+x}MnO_{4+\delta}$ ($0 \leq x \leq 0.5$). The existence of $BaLaMnO_4$ was first reported in 1977 by Benabad et al. [20] together with the first (and only) study reporting on the formation of $Ba_{1+x}La_{1-x}MnO_4$ solid solutions, but a detailed structural analysis on the La-rich series $Ba_{1-x}La_{1+x}MnO_4$ was missing. In $BaLaMnO_4$, Ba^{2+} and La^{3+} are disordered on the A-site and in a nine-fold coordination, while the Mn^{3+} ion is located at the B-site in a tetragonally elongated octahedral geometry. The MnO_6 octahedra are corner-linked in the *ab* plane, while along the *c* axis they are separated by the rock-salt layers. The $3d^4$ ($t_{2g}^3e_g^1$) ion Mn^{3+} (S = 2), subjected to static Jahn-Teller distortions, is situated at the corners of the unit cell lattice forming a square planar magnetic sublattice with 2D sheets extending in the *ab* plane. A certain extent of magnetic frustration is expected due to the stacking sequence of Mn^{3+} layers, as depicted in **Figure 1b**. As mentioned earlier, the magnetic properties of $BaLaMnO_4$ have been unclear for a long period of time until very recently [18] when it was reported that $BaLaMnO_4$ exhibits a spin glass state. Except for $Ba_{0.8}La_{1.2}MnO_{4.1}$ [16] nothing is known about the La-rich phases $Ba_{1-x}La_{1+x}MnO_{4+\delta}$. With the aim of understanding the magnetic properties of these materials, present work reports on the structural and magnetic properties of polycrystalline samples with the $Ba_{1-x}La_{1+x}MnO_{4+\delta}$ composition ($0 \leq x \leq 0.5$) prepared by solid state reactions.

II. EXPERIMENTAL SECTION

1. Synthesis

Polycrystalline $Ba_{1-x}La_{1+x}MnO_{4+\delta}$ samples with $0 \leq x \leq 0.5$ were prepared from La_2O_3 (99.9%), $BaCO_3$ (99.999%), and Mn_2O_3 (99.99%) from CERAC. First, La_2O_3 was pre-fired at 1000 °C to eliminate any residual water. Then stoichiometric amounts of these precursors were homogenised dry, in a ball mill. Pressed rods were placed in a ceramic (alumina) boat and fired in two steps: firstly at 800 °C for 12 h, followed by a second thermal treatment at 1350 °C for 36 h, under Ar to avoid the oxidation of Mn^{3+}. The reactions leading to the formation of $Ba_{1-x}La_{1+x}MnO_{4+\delta}$ samples can be written as follows (**Reaction 1**):

$$(1-x)\ BaCO_3 + (1+x)\ ½\ La_2O_3 + ½\ Mn_2O_3 \rightarrow Ba_{(1-x)}La_{(1+x)}MnO_{4+x/2} + (1-x)CO_2 \uparrow \qquad (1)$$

The temperature and annealing time were found to be the dictating factors in obtaining the targeted phase and to avoid secondary phases. All $Ba_{1-x}La_{1+x}MnO_{4+\delta}$ samples had a black colour.

2. Characterisation

X-ray powder diffraction. Room-temperature powder XRD data was collected (for all samples) with a PANalytical diffractometer equipped with a X'Celerator detector, using Cu-Kα_1 radiation (λ = 1.54056 Å) and a step of 0.0167°. For x = 0.1, 0.2, 0.3, and 0.4, synchrotron diffraction data were also collected at the low energy wiggler beamline of the Brockhouse sector of the Canadian Light Source using a wavelength λ = 0.80441 Å and a Mythen linear position sensitive detector. All structural refinements were performed with Topas R package (version 2.1, Bruker, AXS, Karlsruhe, Germany) which included Lorentzian strain broadening and a TCHZ peak shape function.

Elemental analysis. For the elemental analysis, about 50 mg of each sample was dissolved in 10 mL of hot *aqua regia* following a dilution to 100 mL. An ICPS - inductively coupled plasma spectrometer (Fisher Scientific Instruments, ICP-Varian Vista Pro) was employed for the analyses. Matched standards, i.e. 10 ppm reference solutions of Ba and La in were also used. All elemental analyses were performed with an accuracy of ± 5% of the analyte.

Magnetic measurements. Magnetic susceptibility measurements were conducted using a MPMS SQUID magnetometer (Quantum Design). The direct current (dc) zero-field cooled (ZFC) and field cooled (FC) data were collected in a 2–400 K the temperature range under a

100 Oe applied magnetic field. The samples were placed in gelatine capsules which were held in plastic straws. Two empty gelatine capsules were placed above and below each sample to minimize the noise signal. Also alternating current (ac) magnetic susceptibility measurements were performed in the 2–50 K range at 1, 10, 100, 500, 1000 Hz frequencies and with a 3.5 Oe ac amplitude.

X-ray absorption near edge structure (XANES)

(i) One set of Mn K-edge spectra was collected from $Ba_{0.9}La_{1.1}MnO_{4.05}$ (x = 0.1) and $Ba_{0.7}La_{1.3}MnO_{4+\delta}$ (x = 0.3) samples employing the Sector 20 bending magnet beamline (20-BM; CLS@APS) from the Advanced Photon Source. The beamline was equipped with a Si(111) monochromator. The powder samples were sealed between layers of Kapton tape. Measurements were collected in partial fluorescence and transmission modes. The spectra were collected with a 0.15 eV step size through the edge and were calibrated using Mn metal (6539 eV). The resolution of the Mn K-edge was 0.9 eV.

(ii) The other set of XANES data from $BaLaMnO_4$ and $Ba_{0.6}La_{1.4}MnO_{4+\delta}$ samples as well as reference compounds such as $Mn^{2+}O$, $Mn^{3+}{}_2O_3$, $Mn^{4+}O_2$, and $Ba_{0.8}La_{1.2}Mn^{3+\delta}O_{4+\delta}$ (sample synthesised in oxidising conditions, therefore containing Mn in an oxidation state higher than +3) was collected at ELETTRA, a synchrotron radiation facility in Trieste, Italy. Mn K-edge absorption spectra were measured in transmission mode and at room temperature. Polycrystalline samples were pressed into thin pellets with a total absorption thickness (μd) of 2 above the investigated edge. For these measurements, a Si(111) double-crystal monochromator having an energy resolution of 0.8 eV at 7 keV was employed. The XANES spectra were measured within the interval −250 eV to +1000 eV relative to the Mn K-edge. Energy steps of 0.25 eV each were used with an integration time of 1s/step. To improve the signal-to-noise ratio, three to six repetitions of the scans were superimposed for each sample. The absolute energy reproducibility of the measured spectra was 0.03 eV. A 5 μm thick Mn metal foil was used to determine the exact energy calibration. The Mn K-edge in the Mn metal is positioned at 6539 eV.

Data analysis was performed with the Demeter (IFEFFIT) program package, Athena [21].

Bond valence calculations were carried out according using **Equations 2** and from Brown [22]:

$$S_i = \exp((R_i - R_0)/b) \quad (2)$$

$$V = \sum_i S_i \quad (3)$$

where S_i (the bond valence) is calculated from the R_i and R_0 (bond distance) values. The b parameter is 0.37. Here V (bond valence sum) is the sum of all i bond valences of a particular coordination sphere.

III. RESULTS AND DISCUSSION

1. X-ray powder diffraction

Samples of $Ba_{1-x}La_{1+x}MnO_{4+\delta}$ ($0 \leq x \leq 0.5$) have been obtained as black polycrystalline materials. The laboratory X-ray diffraction patterns are shown in **Figure 2**.

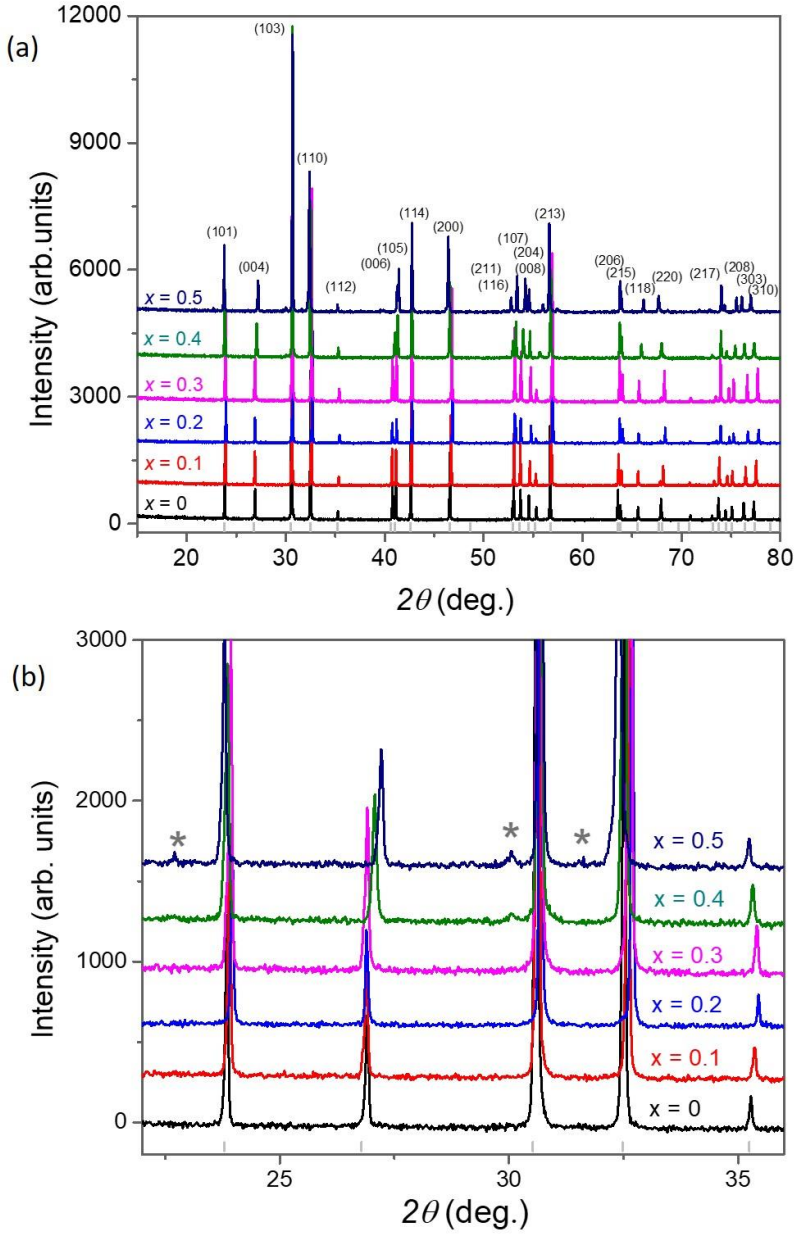

Figure 2 The room-temperature X-ray diffraction patterns for the $Ba_{1-x}La_{1+x}MnO_{4+\delta}$ series (x = 0.1−0.5). The impurity La_2O_3 is marked with *****. The marked 2 theta positions shown below the profile (grey bars) show the allowed Bragg peaks for Cu Kα_1.

All samples crystallize within the *I*4/*mmm* space group with sharp and well-defined reflections – **Figure 2a**. Asymmetric peak broadening was observed for all samples, but it was more pronounced for $x = 0.1$ and 0.3. Such effects have been observed before in layered oxides and are thought to be originating from local defects and/or oxygen interstitials/vacancies [23, 24]. Samples with $x \leq 0.3$ were phase-pure, while samples with $x \geq 0.4$ contained La_2O_3 as a secondary phase, marked with ***** in **Figure 2b**.

Structural refinements were carried out on all samples using the laboratory data and for $0.10 \leq x \leq 0.40$ using the synchrotron data. The results are shown in the Supplemental Material, **Figure S1** and **S2**, and **Tables S1** and **S2** [25].

The unit cell parameters of the $Ba_{1-x}La_{1+x}MnO_{4+\delta}$ series were calculated from laboratory X-ray powder diffraction analysis on $x = 0$ and 0.5, while for $0.10 \leq x \leq 0.40$ using the synchrotron data. For $x = 0$, the $a = 3.9036(1)$ Å, $c = 13.2927(1)$ Å, and unit cell volume, V, is 202.553(3) Å^3. The substitution of Ba^{2+} (1.47 Å) by the smaller La^{3+} ion (1.216 Å) initially leads to a decrease, followed by an increase of a parameter, while the c parameter slightly increases up to $x \leq 0.2$ but decreases for $x > 0.2$ (**Figure 3a** - top). According to **Figure 3a** - bottom, the unit cell volume seems to shrink for $0 \leq x \leq 0.2$ then expands for $x \geq 0.3$.

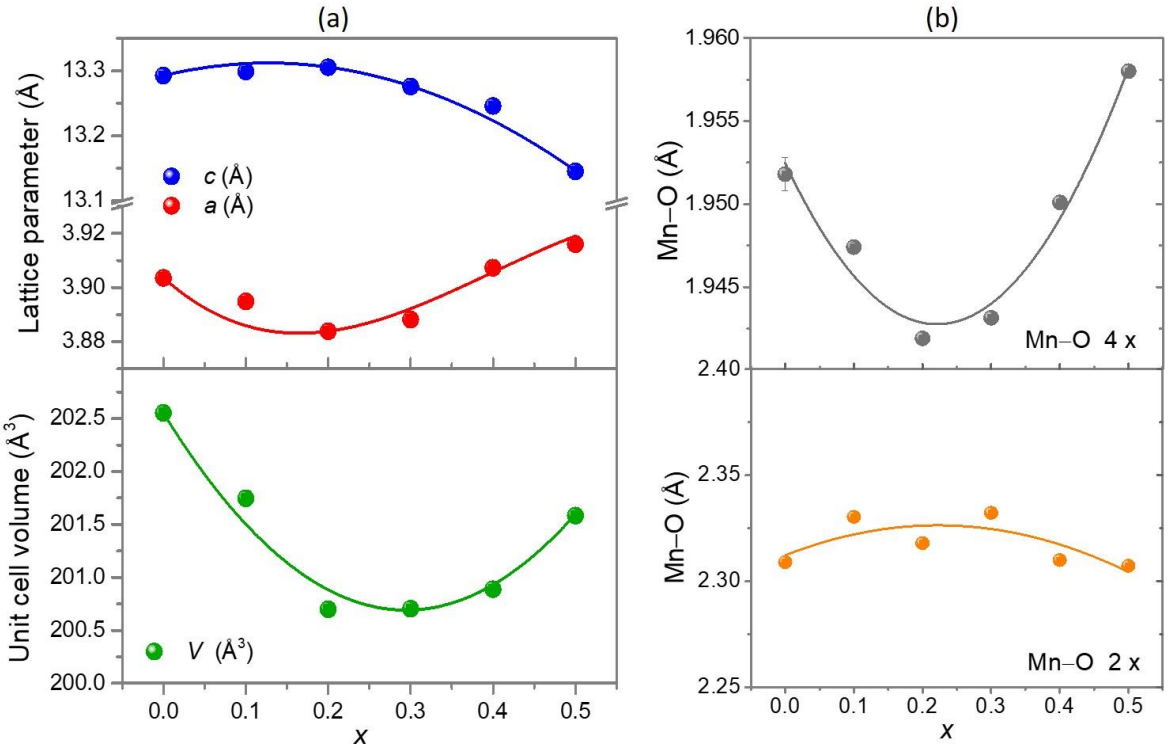

Figure 3 (a) The evolution of the unit cell constants and volume of $Ba_{1-x}La_{1+x}MnO_{4+\delta}$ as a function of x; **(b)** the evolution of the planar and axial Mn–O bonds lengths along the $Ba_{1-x}La_{1+x}MnO_{4+\delta}$ series. The lines are guides to the eye only.

With increasing La concentration, the MnO_6 octahedron experiences a shortening of the Mn–O planar bond lengths from 1.9518(1) Å for $x = 0$ to 1.9494(1) Å for $x = 0.2$, while for $x > 0.2$ there is a linear increase of the Mn–O planar bonds lengths up to 1.9580(3) Å for $x = 0.5$. Moreover, with increasing the La concentration, the axial Mn−O bonds slightly increase from 2.3104(1) Å to 2.3723(1) Å ($0 < x < 0.3$) and remain relatively constant for $x > 0.3$. Furthermore, the elongation of the MnO_6 octahedron leads to an increase of the distortion index, *D.I.* as shown in **Table 1**. The distortion index, *D.I.*, is defined as:

$$D.I. = [<(Mn - O)axial - (Mn - O)equatorial>] / <Mn - O> \quad (2)$$

where <Mn–O> is defined as the average of the axial and equatorial Mn–O distances.

Table 1 The Mn–O bond lengths and the distortion index, *D.I.* for $Ba_{1-x}La_{1+x}MnO_{4+\delta}$ ($0 \leq x \leq 0.5$), and bond valences determined from the bond-valence model. Data for x = 0.1–0.4 were calculated from synchrotron data.

Bond	x **= 0**	x **= 0.1**	x **= 0.2**	x **= 0.3**	x **= 0.4**	x **= 0.5**
Mn–O (planar)	1.9518(1)	1.9474(3)	1.9419(1)	1.9441(1)	1.9501(1)	1.9474(3)
Mn–O (axial)	2.3104(1)	2.3304(3)	2.3157(1)	2.3723(1)	2.3100(1)	2.3304(3)
D.I.	0.173	0.184	0.181	0.205	0.174	0.168
B.V. (Mn)	2.83	2.84	2.89	2.81	2.85	2.80

The compression of the Mn–O planar bonds for $x \leq 0.2$ might be simply a result of the substitution of Ba^{2+} for smaller La^{3+} ion, while for $x > 0.2$ the increase could suggest a decrease in the concentration of Mn^{3+} (ionic radius of 0.645 Å) and a possible admixture with larger Mn^{2+} ion (ionic radius of 0.830 Å).

The slight expansion of Mn−O axial bonds with increasing La content up to about $x = 0.2$ indicates an increase of the Jahn-Teller distortion. This excludes the presence of Mn^{4+} or Mn^{2+} species as they prefer non-distorted octahedral sites. Moreover, it is expected that this would also affect the *d*-orbital energies of the Mn^{3+} in the *ab* plane.

2. Elemental analysis

The ICP method was chosen to investigate the empirical formula of the as-obtained polycrystalline $Ba_{1-x}La_{1+x}MnO_{4+\delta}$ samples. Two compositions were chosen, $BaLaMnO_4$ and $Ba_{0.8}La_{1.2}MnO_{4.1}$. The results are presented in **Table 2**. Both samples analysed showed a Ba/La

ratio almost identical to the nominal ratios of 1.00 for $BaLaMnO_4$ and 0.66 for $Ba_{0.8}La_{1.2}MnO_{4.1}$, respectively, which confirms the stoichiometry of our samples.

Table 2 The results of elemental analysis on polycrystalline $BaLaMnO_4$ and $Ba_{0.8}La_{1.2}MnO_{4.1}$.

Nominal formula	Element				Ba/La ratio	La/Ba ratio	Empirical formula
	Ba		La				
	ppm	ppm/A	ppm	ppm/A			
$BaLaMnO_4$	13.9(6)	0.101(6)	14.1(7)	0.101(7)	1.00(7)	1.00(7)	$BaLaMnO_4$
$Ba_{0.8}La_{1.2}MnO_{4.1}$	7.3(3)	0.053(3)	11.1(5)	0.080(5)	0.663(3)	1.509(5)	$Ba_{0.8}La_{1.2}MnO_{4.1}$

3. XANES analysis

The Mn oxidation state in both $BaLaMnO_4$ (x = 0) and $Ba_{0.8}La_{1.2}MnO_{4.1}$ (x = 0.2) compounds is +3.0(1) as determined from XANES analysis in our previous work [16]. For charge balance, interstitial oxygen was found in the AO layers of the x = 0.2 sample. But will the Mn^{3+} state persist for x > 0.2 or will the oxygen uptake have already reached a maximum? To answer this question, it is therefore very important to find out what is the oxidation state of Mn in the samples with x > 0.2. From the structural study presented in section **III.1**, we do expect that the oxygen uptake should have reached a saturation value and the excess La could now be accommodated by a mixed Mn^{2+} and Mn^{3+} at the Mn site. To shine light on this, Mn-edge XANES analysis on $Ba_{0.6}La_{1.4}MnO_{4+\delta}$ (x = 0.4) was used.

The normalized XANES spectra of Mn in the $Ba_{0.6}La_{1.4}MnO_{4+\delta}$ sample are plotted in **Figure 4**. A set of selected XANES spectra collected on (reference) Mn compounds containing Mn in different valence states but the same oxygen ligands are also plotted. The valence state of Mn in the analysed samples was determined from the shift in energy of the Mn absorption edge relative to reference compounds. The Mn absorption edge is shifted to higher energies with increasing the oxidation state. A shift of about 3.5 eV per unit oxidation state was observed in reference Mn compounds (**Figure 4**) which agrees with previous results [26, 27]. **Figure 4** shows that the Mn K-edge position in the sample with x = 0.4 is shifted to lower energies by −1 eV relative to the Mn^{3+} edge position for samples where Mn is in +3.0(1) oxidation state such as in $Ba_{0.8}La_{1.2}MnO_{4.1}$ and $BaLaMnO_4$. This shift suggests an average oxidation state of Mn of +2.7(1), and therefore, an admixture of Mn^{2+}/Mn^{3+} at the B-site.

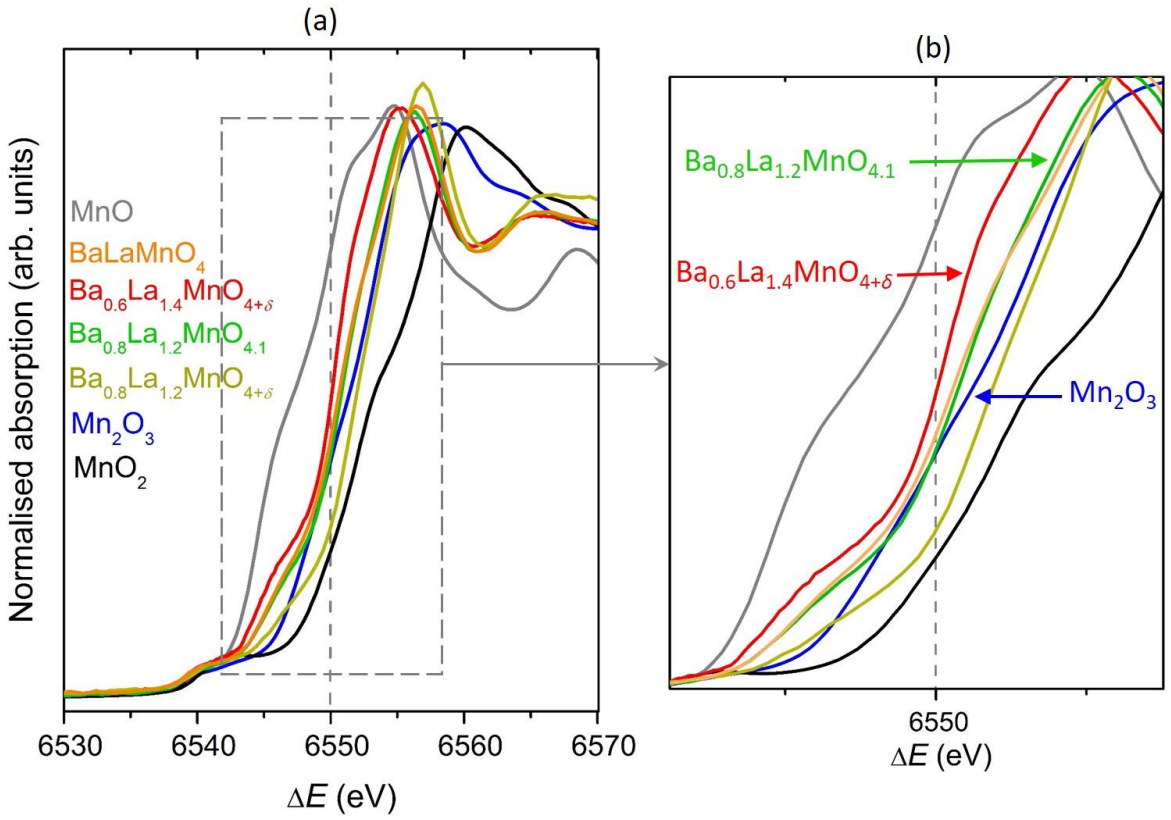

Figure 4 (a) Mn K-edge XANES spectra of $Ba_{0.6}La_{1.4}MnO_{4+\delta}$ and reference compounds containing Mn in different valence states, $Mn^{+2}O$, $Mn_2{}^{+3}O_3$ $BaLaMn^{+3}O_4$, $Ba_{0.8}La_{1.2}Mn^{+3}O_{4.1}$, and $Mn^{+4}O_2$. A vertical dotted line is located at 6550 eV which is the energy of the Mn_2O_3 absorption edge. **(b)** Detail showing the Mn edge in $Ba_{0.6}La_{1.4}MnO_{4+\delta}$ is shifted to lower energy compared to $Ba_{0.8}La_{1.2}MnO_{4.1}$ and Mn_2O_3 reference samples with Mn in +3 oxidation state.

The XANES analysis performed on $Ba_{0.9}La_{1.1}MnO_{4.05}$ (**Figure 5)** revealed that for this composition, Mn exists in a +3.0(1) oxidation state with its absorption edge being positioned between MnO, MnO_2 and at the same position as Mn_2O_3. On the other side, the sample with x = 0.3 ($Ba_{0.7}La_{1.3}MnO_{4+\delta}$) has the absorption edge slightly shifted to lower energies by −0.3 eV relative to the Mn^{3+} edge position for the $Ba_{0.9}La_{1.1}MnO_{4.05}$ and Mn_2O_3 sample where Mn is in +3 oxidation state. This shift suggests an average oxidation state of Mn of +2.9(1).

In conclusion, our XANES results suggest that for the samples with $x > 0.2$, no more oxygen can be accommodated at the interstitials to account for the excess of La, but the charge balance gets satisfied by a reduction of some of the Mn^{3+} ions to Mn^{2+}, which agrees with the structural results in the previous section.

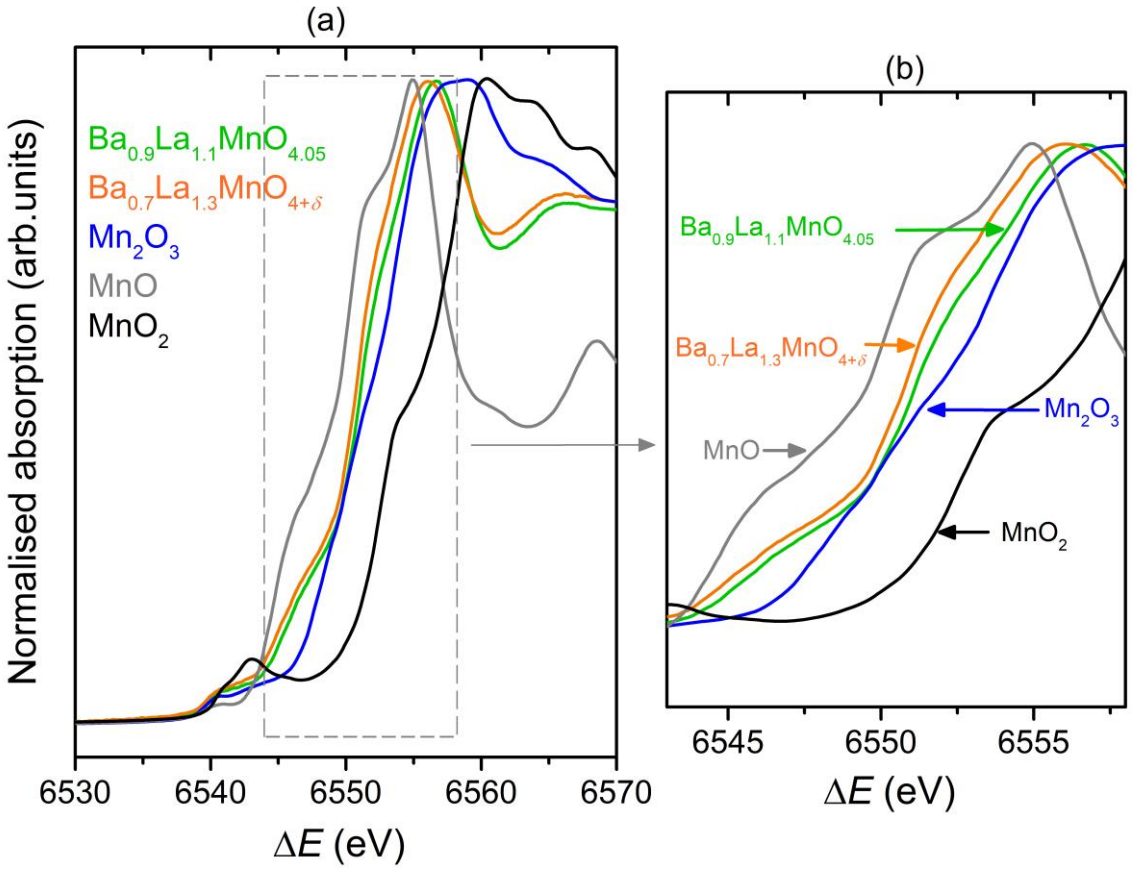

Figure 5 (a) The Mn K-edge XANES spectra of $Ba_{0.9}La_{1.1}MnO_{4.05}$, $Ba_{0.7}La_{1.3}MnO_{4+\delta}$ and reference Mn compounds where Mn is in different valence states ($Mn^{+2}O$, $Mn_2^{+3}O_3$, and $Mn^{+4}O_2$). **(b)** Detail showing the Mn edge in $Ba_{0.7}La_{1.3}MnO_{4+\delta}$ is shifted to lower energy compared to $Ba_{0.9}La_{1.1}MnO_{4.05}$ and Mn_2O_3 reference compounds with Mn in +3 oxidation state.

4. Magnetic properties

The dc magnetic susceptibility data for the polycrystalline $Ba_{1-x}La_{1+x}MnO_{4+\delta}$ ($0 < x < 0.4$) samples are presented in **Figure 6**. It has been previously established that the general shape of the polycrystalline susceptibility curves, especially for ZFC, is diagnostic of the anisotropic spin glass state [16]. For an isotropic spin glass, the ZFC curve falls rapidly below T_g but in the anisotropic case this does not happen as only one of the three spin components freezes while the other two remain dynamic giving rise to a broad maximum well below T_g as well as the cusp at T_g. Similar magnetic behaviour was found for $0 < x < 0.4$, with T_g values dependent on x: T_g = 21.9(4) K for x = 0.1, 26.8(4) K for x = 0.2, 24.1(3) K for x = 0.3, and 20.5(3) K for x = 0.4, respectively. The results for x = 0.0 and 0.2 have been presented previously [16,18], the latter being obtained on a single crystal.

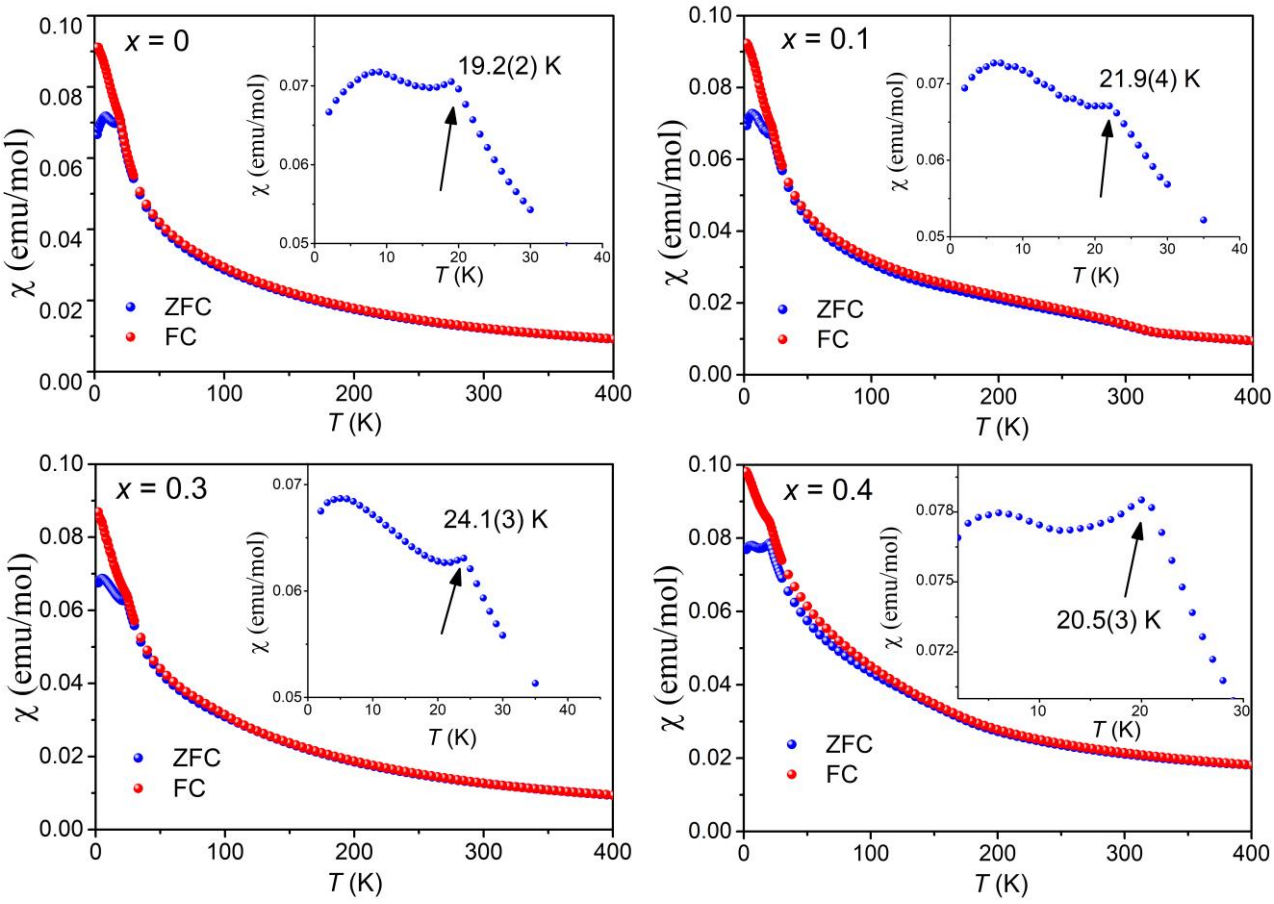

Figure 6 The FC and ZFC dc magnetic susceptibility data for $Ba_{1-x}La_{1+x}MnO_{4+\delta}$ for selected x (x = 0, 0.1, 0.3, and 0.4).

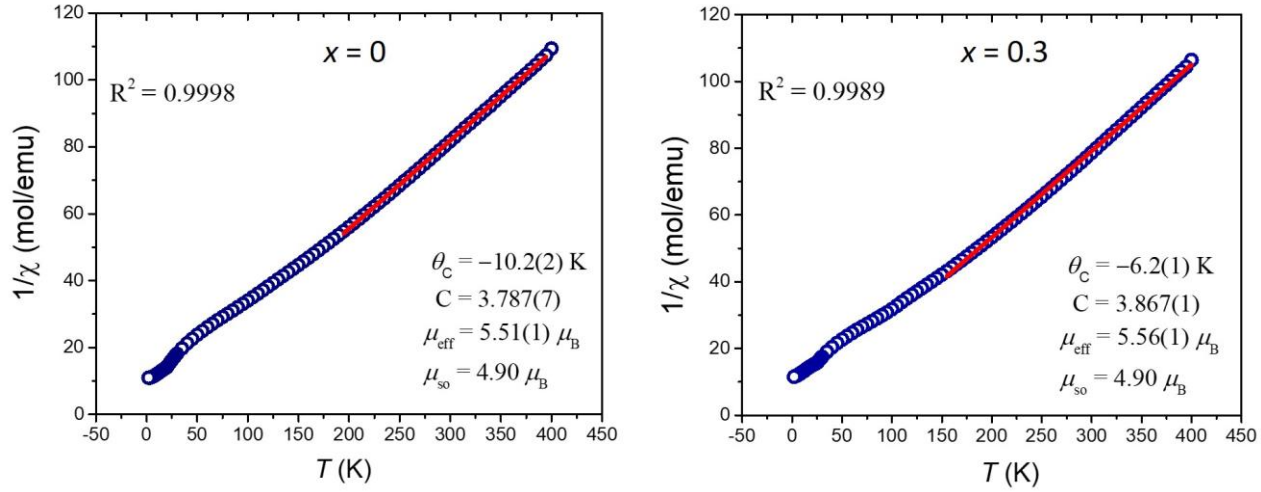

Figure 7 The inverse magnetic susceptibility for selected x (0.0 and 0.3) and their Curie-Weiss fits.

Figure 7 shows the C-W fits to the FC for selected x, i.e., x = 0 and 0.3. We chose to omit x = 0.1 and 0.4 because we noticed a very small effect in the susceptibilities of these two samples

- at about 320 K for x = 0.1 and at 170 K for x = 0.4, respectively, which most likely comes from a very small amount of a ferromagnetic impurity as observed earlier [11]" [11].

The calculated Weiss temperatures in the 200 – 400 K temperature range were found to be: −10.2 K for x = 0 and −3.2 for x = 0.3, respectively. The Curie constants of 3.78 (x = 0) and 3.86 (x = 0.3) gives an effective magnetic moment of 5.5 (x = 0) and 5.6 (x = 0.3) respectively, which are larger than 4.90 μ_B - the spin only value. If the region used for the C-W fit is still influenced by short-range spin correlations, then it is not truly paramagnetic and any C-W fitting parameters would be suspect. The slope of χ^{-1} vs T will change with the T-range selected for the fitting.

Figure 8 summarizes the spin glass transitions in $Ba_{1-x}La_{1+x}MnO_{4+\delta}$ as found from the ac magnetic susceptibility measurements. We find that for $BaLaMnO_4$ the T_g is centred at 21 K for a frequency of 10 Hz but its position and sharpness of the cusp is frequency dependent: it shifts to higher temperatures with increasing the frequency, up to 22.2 K for a frequency of 1000 Hz. These results support the spin glass behaviour observed in the *dc* susceptibility.

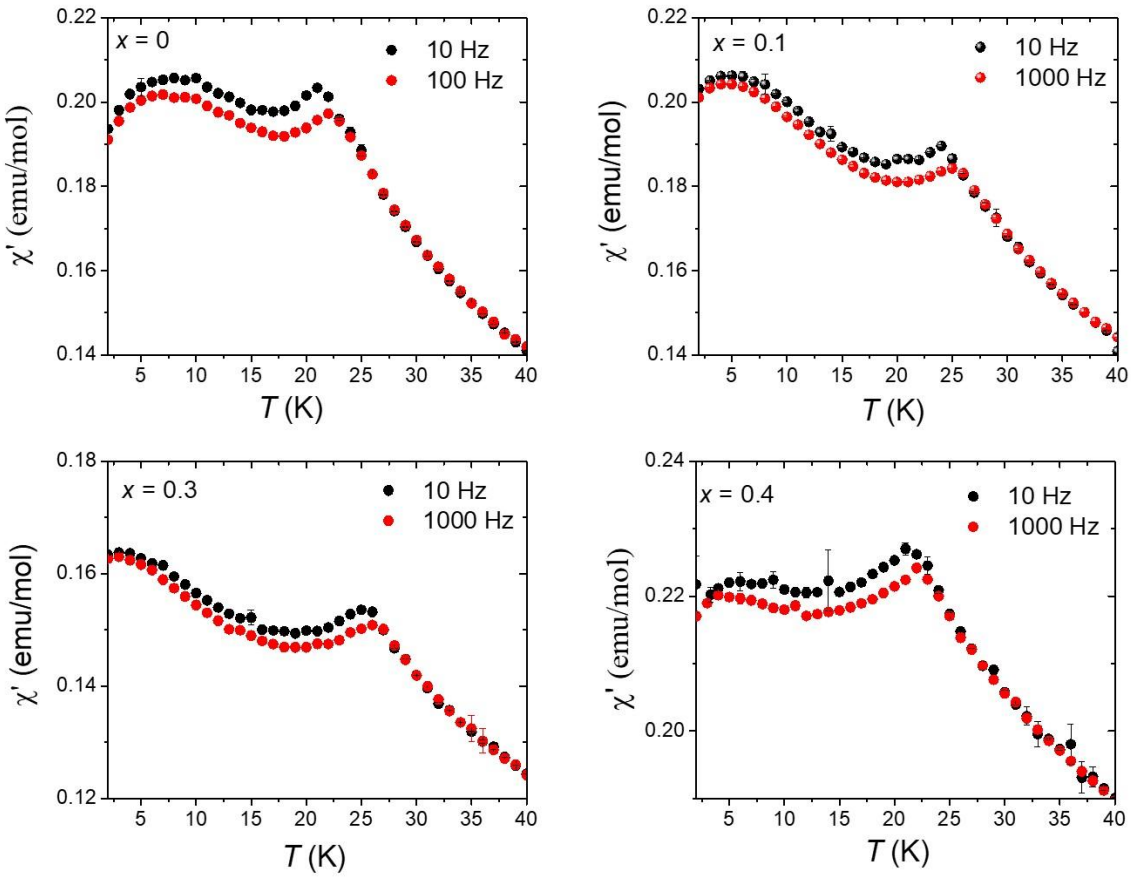

Figure 8 The temperature dependence of the real part (χ') of the *ac* magnetic susceptibility of $Ba_{1-x}La_{1+x}MnO_{4+\delta}$, for selected x (x = 0, 0.1, 0.3, and 0.4), selected frequencies, and zero field.

Figure 9 summarize the spin glass transitions in $Ba_{1-x}La_{1+x}MnO_{4+\delta}$ as found from dc magnetic susceptibility measurements. The glass temperature, T_g increases with x for $0 < x < 0.2$, reaching a maximum for $x = 0.2$, while for $x > 0.2$ T_g experiences a decrease.

The trend in the freezing temperature, T_g, as a function of x could be rationalized based on the structural and compositional changes induced by the La excess (x). With increasing x there is an elongation of the octahedra (Mn-O axial bonds) and a compression of the Mn-O planar bonds up to $x = 0.2$, above which the axial bonds remain constant but Mn-O planar bonds start to expand with x. As well as structural trends, the oxidation state for Mn changes for $x > 0.2$, i.e., a mixed Mn^{3+}/Mn^{2+} state instead of purely Mn^{3+}. This may introduce a weak double exchange to the mix. It is not completely clear how this would decrease T_g. It is worth noting some similarities and differences with the known system $La_{1-x}Sr_{1+x}MnO_4$, $x = 0.2, 0.4, 0.5, 0.6$ [28]. In this case some of the Mn^{3+} ions will be oxidized to Mn^{4+} with increasing x, which will introduce a competing FM interaction via Zener's double exchange [27]. A spin glass state does set in for $x > 0.2$ but the spin freezing is isotropic. Unfortunately, detailed structural information was not presented in ref. [28]. It seems that the substitution of Ba^{2+} with smaller La^{3+} cation causes a decrease of the unit cell volume, a decrease in the Mn-O planar bond lengths, and an increase of the *D.I.* – **Table 1**. A decrease in the Mn-O planar bond lengths is expected to cause an increase in the antiferromagnetic exchange interactions, while the increase of the *D.I.* index might lead to an increase in the ferromagnetic interactions.

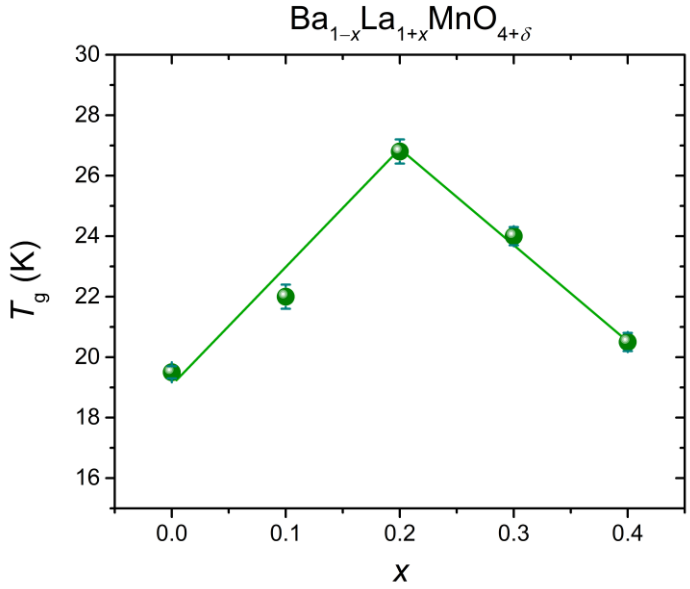

Figure 9 The dependence of the maxima of the maxima in the dc susceptibility for $Ba_{1-x}La_{1+x}MnO_{4+\delta}$, $x = 0$, 0.1, 0.2, 0.3, and 0.4. The lines are just guiding the eye.

IV. CONCLUSIONS

A new family of anisotropic spin glasses, $Ba_{1-x}La_{1+x}MnO_{4+\delta}$ ($0 \leq x \leq 0.4$) with the *I*4/*mmm* space group was synthesised by solid-state reactions. The $x = 0.2$ member, which has been synthesised and obtained as a single crystal in a previous work [16] had only the *c*-axis (*z*) spin component freezing, while the other components remained dynamic. This study investigated compositions with $0 \leq x \leq 0.4$ and revealed that the whole series exhibits anisotropic spin glass behaviour. This is all the more remarkable as the corresponding $Sr_{1-x}La_{1+x}MnO_{4+\delta}$ series members for $x = 0.0$ and 0.2 show long range and short-range antiferromagnetic order [28]. The dc and ac magnetic susceptibility have shown that the spin freezing temperature, T_g varies across the series such that T_g is first increasing for $x \leq 0.2$ reaching a maximum at about $x = 0.2$, but then it shows a decrease for $0.2 < x < 0.4$.

It was also found that for $x \leq 0.2$, Mn^{3+} alone is present, while small levels of Mn^{2+} appear for $x > 0.2$, as revealed by XANES analysis. Therefore, the origin of spin glass state in the $Ba_{1-x}La_{1+x}MnO_{4+\delta}$ series, seems to be different for the two regimes:

a) $\boldsymbol{x \leq 0.2}$: here Mn is in +3 oxidation state only so the origin of the glassy state might be similar as for $BaLaMnO_4$ [18]: competition between the antiferromagnetic and ferromagnetic180º superexchange interactions for the Mn^{3+} ($t_{2g}^3e_g^1$) ion aided by subtle changes in the MO_6 octahedra due to increase in *x* with further consequences on the strength of the antiferromagnetic interaction vs the ferromagnetic interactions and which are reflected on the value of the freezing temperature.

b) $\boldsymbol{0.2 < x < 0.4}$: for this regime, the XANES showed an admixture of Mn^{2+} and Mn^{3+} which might change the origin of the glassy state. For such a mixture, the Goodenough rules [29] predict ferromagnetic interactions via the Mn^{2+} $(d_{x^2-y^2})^1$ – O 2p – Mn^{3+} $(d_{x^2-y^2})^0$ transfer which is a form of the double exchange interaction proposed by Zener [30]. Note that a spin glass behaviour was also observed in the analogue series $La_{1-x}Sr_{1+x}MnO_4$ with $0.2 < x < 0.6$ [28] where the coexistence of Mn^{2+} with Mn^{3+} would give rise to ferromagnetic double exchange interactions to such an extent that they become nearly equal to the antiferromagnetic superexchange interactions, leading to a spin glass state.

Thus, similar as $BaLaMnO_4$ [18] and $Ba_{0.8}La_{1.2}MnO_{4.1}$ [16] also the La-rich phases, $Ba_{1-x}La_{1+x}MnO_{4+\delta}$ ($x = 0.1$, 0.3, and 0.4) exhibit the very rare anisotropic spin glass behaviour with only the *c*-axis spin component freezing below T_g, although the origin of frustration is dependent on *x*.

ACKNOWLEDGEMENTS

M. Dragomir and J. E. Greedan acknowledge Natural Sciences and Engineering Research Council (NSERC), Canada, for the financial support in form of a Discovery Grant.

I. Arčon would like to acknowledge the access to synchrotron radiation facilities of ELETTRA, XAFS beamline, Trieste, Italy, project 20170045. Part of this his research was supported by the Slovenian Research Agency (P1-0112 and P2-0105) and project CALIPSO plus under the Grant Agreement 730872 funded by HORIZON 2020.

Sector 20 (CLS@APS) facilities at the Advanced Photon Source (APS) are supported by the US Department of Energy - Basic Energy Sciences, the Canadian Light Source and its funding partners, and the APS. Use of the APS, an Office of Science User Facility operated for the U.S. Department of Energy (DOE) Office of Science by Argonne National Laboratory, was supported by the U.S. DOE under Contract No. DE-AC02-06CH11357.

A part of the research described in this manuscript was performed at the Canadian Light Source, a national research facility (CLS) of the University of Saskatchewan, supported by the Canada Foundation for Innovation (CFI), the Canadian Institutes of Health Research (CIHR), the Government of Saskatchewan, and the University of Saskatchewan. G. King would like to thank Adam Leontowich for assistance with the powder diffraction measurements.

References

1 S. Jin, T. H. Tiefel, M. McCormack, R. A. Fastnacht, R. Ramesh, L. H. Chen, Thousand-fold Change in Resistivity in Magnetoresistive La-Ca-Mn-O Films, Science **264**, 413–415 (1994).

2 K.-I. Chahara, T. Ohno, M. Kasai, Y. R. Kozono, Magnetoresistance in magnetic manganese oxide with intrinsic antiferromagnetic spin structure, Appl. Phys. Lett. **63**, 1990–1992 (1993).

3 Y. Moritomo, A. Asamitsu, H. Kuwahara, Y. Tokura, Giant magnetoresistance of manganese oxides with a layered perovskite structure, Nature **380**, 141–144 (1996).

4 D. Balz, Uber die Struktur des K_2NiF_4, Naturwissenchaften **40**, 241–241(1953).

5 B. Brehler, H. G. Winkler, Struktur des K_2MgF_4, Heilderberger Beiträge zur Mineralogie und Petrographie **4**, 6–11 (1954).

6 J. D. Jorgensen, B. Dabrowski, S. Pei, D. G. Hinks, L. Soderholm, B. Morosin, J. E. Schirber, E. L. Venturini, Ginley, Superconducting phase of $La_2CuO_{4+\delta}$: A superconduction composition resulting from phase separation, Phys. Rev. B **38**, 11337–11345 (1988).

7 J. D. Jorgensen, B. Dabrowski, S. Pei, D. G. Hinks, Structure of the interstitial oxygen defect in $La_2NiO_{4+\delta}$, Phys. Rev. B. **40**, 2187–2199 (1989).

8 D. E. Rice, D. J. Buttrey, An X-ray Diffraction Study of the Oxygen Content Phase Diagram of $La_2NiO_{4+\delta}$, J. Solid State Chem. **105**, 197–210 (1993).

9 S. Kawano, N. Achiwa, N. Kamegashira, M. Aoki, Magnetic properties of K_2NiF_4 type oxides, $SrLaMnO_{4+x}$ ($0 \leq x \leq 0.2$), J. Phys. **49**, C8–829 (1988).

10 S. Larochelle, A. Mehta, L. Lu, P. K. Mang, O. P. Vajk, N. Kanero, J. W. Lynn, L. Zhou, M. Greven, Structural and magnetic properties of the single-layer manganese oxide $La_{1-x}Sr_{1+x}MnO_4$, Phys. Rev. B **71**, 024435 (2005).

11 M. Bieringer, J. E. Greedan, Structure and magnetism in $BaLaMnO_{4+/-\delta}$ ($\delta = 0.00, 0.10$) and $Ba_xSr_{1-x}LaMnO_4$. Disappearance of magnetic order for $x > 0.30$, J. Mater. Chem. **12**, 279–287 (2002).

12 A. Collomb, D. Samaras, J. C. Joubert, Determination of magnetic structures of $SrCrO_4$ compounds using neutron diffraction, Phys. Status Solidi A **50**, 635–642 (1978).

13 S. E. Dann, M. T. Weller, D. Currie, M. F. Thomas, A. D. Al-Rawwas, Structure and Magnetic properties of Sr_2FeO_4 and $Sr_3Fe_2O_7$ studied by neutron powder diffraction and Mossbauer spectroscopy, J. Mater Chem. **3**, 1231–1237 (1993).

14 K. Nakajima, K. Yamada, S. Hosoya, Y. Endoh, M. Greven, R. J. Birgeneau, Spin dynamics and spin correlations in the spin $S = 1$ two-dimensional square-lattice Heisenberg antiferromagnet La_2NiO_4, Z. Phys. B **96**, 479–489 (1995).

15 T.-H. Kao, H. Sakurai, T. Kolodiazhnyi, Y. Suzuki, M. Okabe, T. Asaka, K. Fukuda, S. Okubo, S. Ikeda, S. Hara, T. Sakurai, H. Ohta, H.-D. Yang, Crystal structure and physical properties of Cr and Mn oxides with $3d^3$ electronic configuration and a K_2NiF_4-type structure, J. Mater. Chem. C **3**, 3452–3459 (2015).

16 M. Dragomir, P. A. Dube, I. Arčon, C. Boyer, M. Rutherford, C. Wiebe, G. King, H. Dabkowska, J. E. Greedan, Comparing Magnetism in Isostructural Oxides $A_{0.8}La_{1.2}MnO_{4.1}$: Anisotropic Spin Glass (A = Ba) Versus Long Range Order (A = Sr), Chem. Mater. **31**, 7833–7844 (2019).

17 M. Dragomir, *to be published*.

18 M. Bieringer, J. R. Steward, A. P. Grosvenor, M. Dragomir, J. E. Greedan, Quenching of long-range order and the Mn^{3+} ordered moment in the layered antiferromagnet, $Ba_xSr_{1-x}LaMnO_4$: a polarized neutron scattering study, Inorg. Chem. **58**, 4300–4309 (2019).

19 U. Atzmony, E. Gurewitz, M. Melamud, H. Pinto, Anisotropic spin-glass behaviour in Fe_2TiO_5, Phys. Rev. Lett. **43**, 782–785 (1979).

20 A. Benabad, A. Daoudi, R. Salmon, G. Le Flem, Les phases Sr*Ln*MnO_4 (*Ln* = La, Nd, Sm, Gd), Ba*Ln*MnO_4 (*Ln* = Sr, Ba) et $M_{1+x}La_{1-x}MnO_4$ (*M* = Sr, Ba), J. Solid State Chem. **22**, 121–126 (1977).

21 B. Ravel, M. Newville, ATHENA, ARTEMIS, HEPHAESTUS: data analysis for X-ray absorption spectroscopy using IFEFFIT, J. Synchrotron Radiat. **12**, 537–541 (2005).

22 I. D. Brown, *The Chemical Bond Inorganic Chemistry*. *The Bond valence Model*, 2nd edition, Oxford University Press, 2016.

23 T. Broux, C. Prestipino, M. Bahout, O. Hernandez, D. Swain, S. Paofai, T. C. Hansen, C. Greaves, Unprecedented High Solubility of Oxygen Interstitial Defects in $La_{1.2}Sr_{0.8}MnO_{4+\delta}$ up to $\delta \sim 0.42$ Revealed by In Situ High Temperature Neutron Powder Diffraction in Flowing O_2. Chem. Mater. 25, 4053–4063 (2013).

24 J. Rodriguez-Carvajal, M. T. Fernandez-Diaz, J. L. Martinez, Neutron diffraction study on structural and magnetic properties of La_2NiO_4. J. Phys.: Condens. Matter 3, 3215–3234 (1991).

25 See Supplemental Material at [URL] for X-ray diffraction patterns and detailed structural parameters obtained from Rietveld refinement analysis.

26 T. Ressler, J. Wong, J. Roos, Manganese speciation in exhaust particulates of automobiles using MMT-containing gasoline, J. Synchrotron Radiat. **6**, 656–658 (1999).

27 R. Dominko, C. Sirisopanaporn, C. Masquelier, D. Hanzel, I. Arcon, M. Gaberscek, On the origin of the electrochemical capacity of $Li_2Fe_{0.8}Mn_{0.2}SiO_4$, J. Electrochem. Soc. **157**, A1309–A1316 (2012).

28 Y. Marimoto, Y. Tomioka, A. Asamitsu, Y. Tokura, Y. Matsui, Magnetic and electronic properties in the hole-doped manganese oxides with layered structures: $La_{1-x}Sr_{1+x}MnO_4$, Phys. Rev. B **51**, 3297−3300 (1995).

29 J. B. Goodenough, Theory of the Role of Covalence in the Perovskite-type Manganites [La, M(II)]MnO_3, Phys. Rev. **100**, 564–573(1955).

30 C. Zener, Interaction between the *d*-Shells in the Transition Metals. II. Ferromagnetic Compounds of Manganese with Perovskite Structure, Phys. Rev. **82**, 403–405 (1951).